Microgravity Science and Technology (2020) 32:1039–1048
https://doi.org/10.1007/s12217-020-09831-x

ORIGINAL ARTICLE

Dynamic Behavior in a Storage Tank in Reduced Gravity Using Dynamic Contact Angle Method

Ji-Cheng Li[1,2] · Hai Lin[1] · Kai Li[1,2] · Jian-Fu Zhao[1,2] · Wen-Rui Hu[1]

Received: 30 March 2020 / Accepted: 9 September 2020 / Published online: 25 September 2020

Abstract

The oscillation of liquid/gas free surface in a partially filled storage tank caused by an abrupt drop of gravity level is of critical importance for the fluid management in space. In the present study, the dynamic behavior of free surfaces in a model tank (tube) is numerically investigated using volume of fluid (VOF) method in the context of dynamic contact angle (DCA) model. It is concluded that the dynamic behavior of free surface could be captured pretty well using the selected DCA model, as shown by comparison with the results of Drop Tower Beijing experiment. The temporal evolution of free surface reproduces exactly the characteristics of damping oscillations. The detailed dynamic deflections of meniscus reveal crucial dependency between the oscillation frequency of free surface and the boundary condition in the contact line. The oscillation frequency increases when the range of the moving contact line transfers from the spherical-shaped part to the cylindrical part of the tank and maintains constant when the moving contact line remains always at the cylindrical part of the tank. Meanwhile, the oscillation amplitude decreases in line with the increase of oscillation frequency.

Keywords Storage tank · Dynamic behavior · Oscillation frequency · Microgravity · Dynamic contact angle · Liquid sloshing

Introduction

Storage tank is one of the basic components for spacecrafts, in which the behavior of liquid is mostly responsible for the safety, stability, fuel supply and so on. Correspondingly, researchers pay close attentions to the shape of free surface (Kulev and Dreyer 2010; Park et al. 2015; Zhou et al. 2016; Zwicke et al. 2017), the pressure control inside a tank (Lopez et al. 2008; Barsi and Kassemi 2013; Chen and Liang 2013; Kassemi and Kartuzova 2016), the liquid sloshing (Zhou and Huang 2015; Deng and Yue 2017), and the measurement of the residual liquid. The hotspot of researchers has been transferred from the properties of fluids, such as SF 0.65, SF 1.00, FC-77 (Stange et al. 2003), LH_2 (Kumar et al. 2007), to the outer geometry structure (with empty internal structure) of the tank (Lopez et al. 2007) with emphasis laid on capillary flows, especially when a partially filled capsule tank was involved (Kassemi and Kartuzova 2016). Among these studies, the dynamic evolution of the free surface of liquid inside a tank is the key topic, which is principally determined by the surface tension force in a microgravity environment.

The problem related free surface is always coupled with the dynamic behavior of contact line or wettability, which has been widely studied by numerous researchers, with focus concentrated on the droplet impact like problems (Josserand and Thoroddsen 2016; Liang and Mudawar 2017; Quetzeri-Santiago et al. 2019). The commonly used numerical methods addressing multiphase flows with the free surface are the volume of fluid (VOF) (Hirt and Nichols 1981; Gueyffier et al. 1999) and level-set (LS) (Sussman et al. 1994) methods. Generally speaking, the dynamic evolution of interface in a confined container (tank) can be satisfactorily investigated with existing numerical simulation methods.

This article belongs to the Topical Collection: The Effect of Gravity on Physical and Biological Phenomena
Guest Editor: Valentina Shevtsova

✉ Kai Li
likai@imech.ac.cn

✉ Jian-Fu Zhao
jfzhao@imech.ac.cn

[1] Key Laboratory of Microgravity (National Microgravity Laboratory), Institute of Mechanics, Chinese Academy of Sciences, Beijing 100190, China

[2] School of Engineering Science, University of Chinese Academy of Sciences, Beijing 100049, China

Importantly, what intimately associated with the free surface in a storage tank is sloshing, which is a common motivation in space fluid management. A good number of works have covered the sloshing behavior, both experimentally and numerically, such as the Sloshsat FLEVO project (Vreeburg 1999; Dalmon et al. 2018), the Control of Fluid with Vibrations (CFVib) in microgravity (Fernandez et al. 2017; Salgado Sanchez et al. 2019), and the FLUIDICS experiment in the International Space Station (ISS) (Dalmon et al. 2019). As is known, one of the key parameters describing the capillary phenomena is the Bond number defined as $Bo = (\rho_l - \rho_g)g\ell^2/\sigma$, where ρ_l is the density of liquid, ρ_g the density of gas, g the gravity acceleration, ℓ the characteristic length and σ the coefficient of surface tension. Considering the reduced/micro-gravity situation in which the value of g is small, the Bond number becomes very small in space. Therefore, the surface tension will dominate the dynamic behavior of the free surface, as shown by Stange et al. (2003) in their experimental and numerical study on the dynamics of capillary-driven flows of perfectly wetting liquids in circular cylindrical tubes under microgravity condition. Ho and Rahman (2005) extended the numerical simulation of tank to three-dimensional cases and described the difference between two (axisymmetric) and three-dimensional results. Fries and Dreyer (2008) presented an analytic solution for the momentum balance of a liquid and investigated the initial moments of the capillary rise of liquids in a capillary tube. Li et al. (2017) numerically investigated the capillary flow in fan-shaped asymmetric interior corner under microgravity with the effect of contact angle taken into account. The influences of filling level on the sloshing frequency (Li et al. 2018; Yang et al. 2019) and damping ratio (Utsumi 2017) were compared in the low Bond number condition. Despite its fundamental importance, our understanding of the liquid sloshing in a tank remains limited, in part due to the working environment of tank. Specifically, the research works on the behavior of liquid in a tank with geometrical capsule structure under microgravity condition are still not sufficient. In addition, the dynamic contact angle (DCA), caused by contact angle hysteresis, plays a crucial role in the spreading of liquids on solid surfaces as systematically discussed in (Cox 1986). The relationship between DCA and the moving contact line (MCL) is what matters most (Snoeijer and Andreotti 2013; Sui et al. 2014). A good many studies involving MCL or interface problems have adopted different DCA models in their works, such as the droplet impact on surface in supercooled environment (Chang et al. 2019), the droplet behavior in microchannel (Wang et al. 2019), the splashing of droplet onto a surface (Almohammadi and Amirfazli 2019; Quetzeri-Santiago et al. 2019). Furthermore, Blake and Batts (2019) experimentally investigated the relationship between temperature and DCA. The results show that, at the molecular-scale, dynamic wetting is a thermally-activated rate process and the influence of temperature on DCA are not restricted to its effect on surface tension and viscosity. Fricke et al. (2019) theoretically analyzed the MCL problem for two-phase incompressible flows in a kinematic approach and found that the derivative of the contact angle could be expressed in terms of the velocity gradient at the solid wall. Viola et al. (2018) incorporated a nonlinear contact line model where a steep dynamic hysteresis range was adopted into an asymptotic analysis of the sloshing dynamics in a circular cylinder in partial wetting conditions. It was shown that the damping effect of contact line was nonlinearly dependent on the amplitude of motion.

In our previous study (Li et al. 2018), the behavior of liquid in a partially filled capsule storage tank in microgravity condition was studied both numerically and experimentally. As shown in Fig. 1, a sealed and inverted test tube partially filled with water was used to simulate the liquid behavior inside a capsule tank after an abrupt drop of gravity during the short-term microgravity (~3.6 s of duration) by utilizing the Drop Tower Beijing ($10^{-3}g_0$ gravity level with the single capsule mode, g_0=9.807 m/s^2 is the terrestrial gravity acceleration). The dynamic behavior of the free surfaces was studied, and the influences of air fraction and tank diameter on the oscillations of the free surfaces were also discussed. As depicted in Fig. 2, the numerical prediction can capture the averaged characteristic oscillation frequency of the first several major free surface deflections in the experiment. However, major discrepancies were found in the final equilibrium position and the damping intensity. To account for the discrepancies between the numerical and the experimental results, a revised numerical simulation was conducted in the present study. The influences of the contact angle, both the static and dynamic contact angles, and the actual gravity level evolution during the short-term microgravity by utilizing the Drop Tower Beijing were taken into consideration. The revised numerical results are found in good agreement with the experimental results presented in Li et al. (2018). Moreover, the influences of the air fraction (i.e. the boundary condition of the MCL) on the dynamic behavior of the free surface have also been accounted for by taking the above factors into consideration.

Numerical Model

Governing Equations

The volume of fluid (VOF) method (Hirt and Nichols 1981; Gueyffier et al. 1999) was adopted to simulate the dynamic behavior of interfaces in a model tank (tube).

Considering water and air as incompressible fluids, the continuity equation is

$$\nabla \cdot \boldsymbol{u} = 0, \tag{1}$$

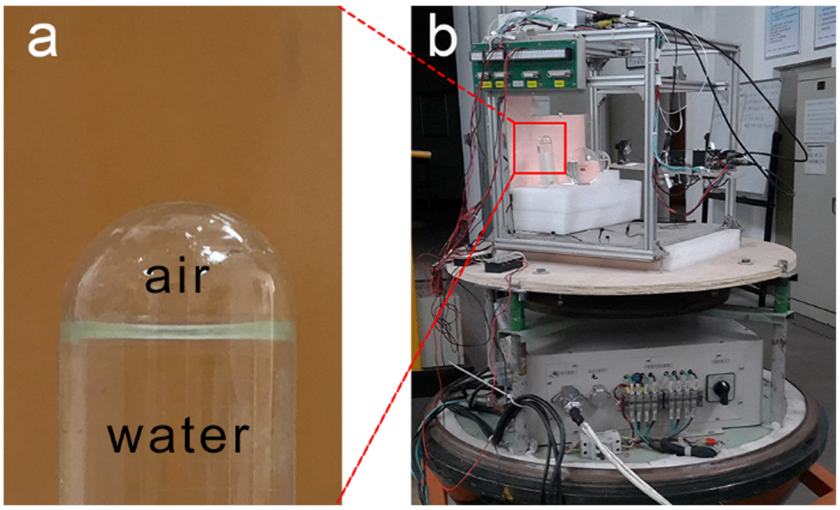

Fig. 1 Experimental apparatus. (a) The cylindrical tube used in experiment. (b) The overall test apparatus (Li et al. 2018)

The governing differential equation of the volume fraction α is

$$\partial_t \alpha + (\boldsymbol{u} \cdot \nabla)\alpha = 0, \tag{2}$$

The momentum conservation equation is as follows:

$$\partial_t(\rho \mathbf{u}) + \nabla \cdot (\rho \boldsymbol{u}\boldsymbol{u}) = -\nabla p + \nabla \cdot (2\mu \mathbf{D}) + \rho \mathbf{g} + \boldsymbol{f}_s, \tag{3}$$

where $\boldsymbol{u}$ is the velocity vector, $\boldsymbol{g}$ the acceleration of gravity, p the pressure, μ the dynamic viscosity, $\boldsymbol{D}$ the rate of deformation tensor defined as $\boldsymbol{D} = (\nabla \boldsymbol{u} + \nabla \boldsymbol{u}^T)/2$. The surface tension force $\boldsymbol{f}_s = 2\sigma_{ij}\rho\kappa_i \nabla \alpha_i/(\rho_i + \rho_j)$. The curvature κ can be calculated by the gradients of the unit normal vector of the two-phase interface as $\kappa = -\nabla \cdot \hat{\boldsymbol{n}}$. The unit normal vector $\hat{\boldsymbol{n}} = \nabla\alpha/|\nabla\alpha|$. The subscript i, j stands for the i, j th phase.

The volume fraction averaged density ρ and dynamic viscosity μ are defined by

$$\rho = \alpha\rho_1 + (1-\alpha)\rho_2, \tag{4}$$

$$\mu = \alpha\mu_1 + (1-\alpha)\mu_2. \tag{5}$$

The piecewise-linear method was used for the reconstruction of the interface (Youngs 1982). Classical PISO solver was adopted for numerical simulation.

Dynamic Contact Angle

Dynamic contact angle (DCA) model considering the contact angle hysteresis originates from the differences between the ideal and real surfaces. It shows a type of saturation function of the contact angle with respect to the capillary number $Ca = \mu u/\sigma$, where u is characteristic velocity. The curves of different DCA models of water are shown in Fig. 3. The model of Hoffman (1975) for small Ca is

$$\theta_D^3 - \theta_e^3 = c_T Ca, \tag{6}$$

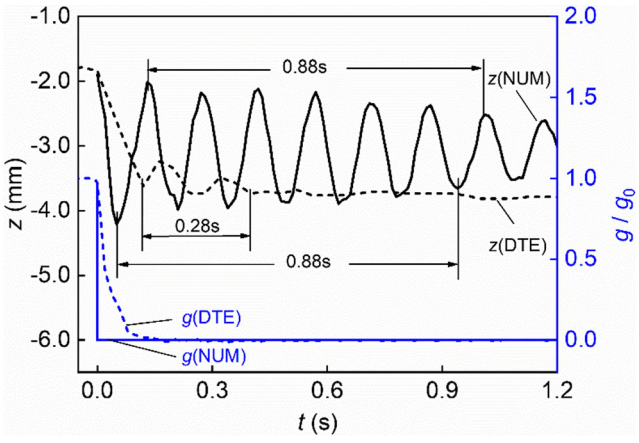

Fig. 2 Comparison of the experimental and numerical results of the evolutions of the center point of free surface in the tube ($d = 21.8$ mm) after an abrupt drop of gravity (Li et al. 2018). The NUM stands for the numerical result and DET for the Drop Tower experimental result

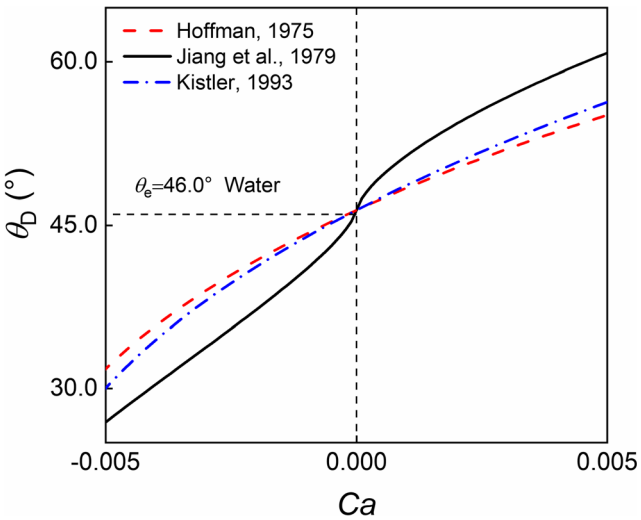

Fig. 3 Variation of DCA as a function of Ca for different DCA models

where θ_D is the dynamic contact angle, θ_e is the static contact angle, c_T is a constant given to be 72 (Hoffman 1975). Jiang et al. (1979) proposed an empirical correlation as

$$\frac{\cos\ (\theta_e)-\cos\ (\theta_D)}{\cos\ (\theta_e)+1}=\tanh\left(4.96Ca^{0.702}\right), \tag{7}$$

and Kistler (1993) proposed a derived DCA formula as

$$\theta_D=f_{\mathrm{Hoff}}\left[Ca+f_{\mathrm{Hoff}}^{-1}(\theta_e)\right], \tag{8}$$

$$f_{\mathrm{Hoff}}(x)=\arccos\left\{1-2\tanh\left[5.16\left(\frac{x}{1+1.31x^{0.99}}\right)^{0.706}\right]\right\}. \tag{9}$$

For the oscillations of free surface in a tank in the present study, the characteristic time and velocity can be selected as $t_c\sim\sqrt{\rho R^3/\sigma}$ and $u_c\sim\sqrt{4\sigma/\rho R}$, where R is the radius of the tube. The calculated value of u_c and t_c are 0.164 m/s and 0.13 s. The capillary number corresponding to u_c is Ca = 0.002, which is of the order of 10^{-3}.

As shown in Fig. 3, the DCA described by Hoffman and Kistler shows little difference as compared with the model proposed by Jiang et al. (1979), and thus the commonly used DCA model of Kistler (1993) was adopted in the present work.

Geometry, Initial and Boundary Conditions

The transient axisymmetric model was adopted for numerical simulation of the dynamic behavior of liquid water in an inverted tube that is employed to model a half-capsule storage tank, as shown in Fig. 4. The inner diameter of the tube d in the simulation model is 21.8 mm which is the same size in the experiment of Li et al. (2018). The height of the straight cylindrical part of the tube, H, was selected to be two times of the diameter in the computational domain. Further increase of H exhibited no influence on the dynamic behavior of liquid.

The boundary on the wall of the tube was divided into two parts to apply different conditions. For the moving contact line region, the Navier-slip boundary condition

$$u=\lambda\hat{\boldsymbol{n}}_w\cdot\nabla u \tag{10}$$

was used, where u is the value of the tangent velocity parallel to the wall, $\hat{\boldsymbol{n}}_w$ is the unit vector normal to the wall, λ is the slip length. According the Hoffman's experiment (Cox 1986), the value of λ is taken as 10^{-6} m, which is of the order of the first layer height of the grid on the wall. The no-slip and no-penetrating boundary condition $u=v=0$, where v is the normal velocity component to the wall, were applied on the wall of the tube except for the moving contact line region. For the

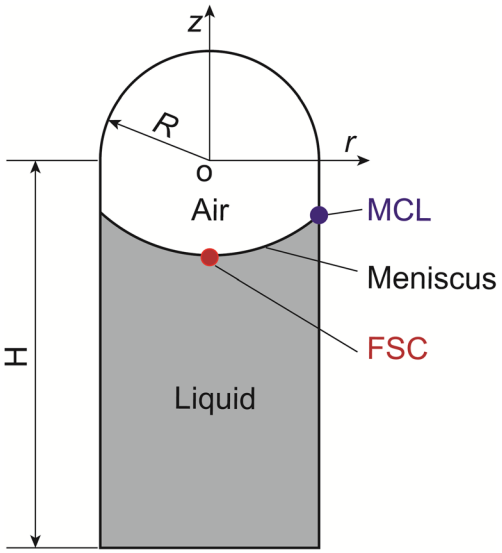

Fig. 4 Schematics of the physical model. The free surface center (FSC) and moving contact line (MCL) are the characteristic points selected to represent the dynamic behavior of the free surface

entire wall, the boundary condition for pressure p and volume fraction α are

$$\left.\frac{\partial p}{\partial n}\right|_w=0,\quad \left.\frac{\partial \alpha}{\partial n}\right|_w=0, \tag{11}$$

i.e. their normal gradient to the solid wall is zero.

The effect of contact angle is described by the wall adhesion model in the following form (Brackbill et al. 1992):

$$\hat{\boldsymbol{n}}=\hat{\boldsymbol{n}}_w\cos\theta_w+\hat{\boldsymbol{t}}_w\sin\theta_w, \tag{12}$$

where $\hat{\boldsymbol{t}}_w$ is the unit vector tangential to the wall. θ_w is the contact angle, i.e. the dynamic contact angle θ_D.

The DCA model is implemented as follows. First, calculate the value of capillary number Ca based on the velocity obtained from the last time step using Eq. (10). Secondly, calculate the value of DCA θ_D using Eq. (8) and (9). Thirdly, apply the contact angle boundary condition given by as Eq. (12). Thus, a time step iteration was completed.

The tube model was initially patched with the water in agreement with the volume fraction of water in the experiments (Li et al. 2018). The equilibrium position of the free surface in normal gravity was calculated based on the initialized flat free surface and taken as the initial condition for the successive calculation in microgravity.

In the numerical simulation, the quadrilateral mesh was adopted and the independence of mesh was checked. The final optimal mesh number was 63,404 in the following study. The range of time interval was 10^{-4} s ~ 10^{-5} s to ensure the Courant number lower than 0.1. The convergence criterion of relative residual error was 10^{-6} for every parameter.

Results and Discussion

Dynamic Behaviors of the Free Surface

Figure 5 shows the dynamic behavior of the free surface deflections in a tube after an abrupt drop of gravity in the case where the air fraction k_v= 1.20. Here, k_v is defined as $k_v = 2V_a/V_0$, where V_a and V_0 are the volume of air and sphere, respectively, and $V_0 = 4\pi R^3/3$. Two kinds of gravity changes are used in the present numerical simulation, one is the idealized step reduction of terrestrial gravity from one to zero (labelled as g_S), and the other is the actual experimental gravity change during the free fall in the Drop Tower Beijing, shown in Fig. 2 (labelled as g_R). The static and dynamic contact angle models are also compared. Considering the principle of light projection and the refraction effect of light near the wall, it is more appropriate to take the FSC points from the lower boundary in the centerline of the tube and the triple phase points from the upper boundary of the shadow on the side of the tube. Therefore, a revised value of the SCA θ_e= 46.0°, rather than the previous value of 55.6° in Li et al. (Li et al. 2018), is obtained based on the experimental observation (see Fig. 6), and is adopted in the present simulation. The same method with Li et al. (2018) was used to construct the free surface profile to obtain the revised value of SCA. Assuming a spherical free surface in microgravity condition, the contact angle θ_e can be calculated by $\theta_e = \arccos(R/R_m)$,where R is the inner radius of test tube and R_m the radius of meniscus. The previous numerical result with a SCA of θ_e= 60.0° in Li et al. (Li et al. 2018) is also included for comparison.

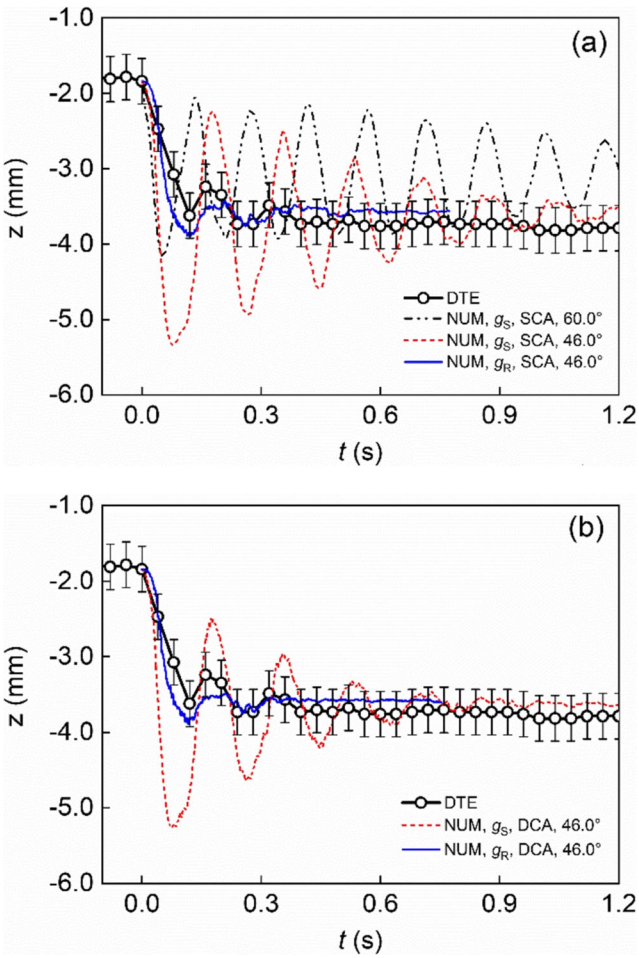

Fig. 5 Temporal evolution of FSC for different physical conditions. (a) SCA model vs. DTE results, (b) DCA model vs. DTE results. The g_S corresponds to the step reduction of terrestrial gravity from one to zero, and the g_R to the actual experimental gravity change in the Drop Tower Beijing, shown in Fig. 2. The error bar is the space uncertainty of the FSC in the Drop Tower experiment with the value of ±0.3 mm

In the Drop Tower experiments, the free surface shows a maximum deflection after the abrupt gravity drop, and the free surface evolution exhibits a rapid damping oscillation to its equilibrium state. For the numerical results with the step reduction of gravity, the case with the SCA of θ_e= 60.0° shows much weaker damping effect on the free surface oscillations with significant discrepancies in the final equilibrium position. When the revised SCA of θ_e= 46.0° was adopted, the free surface evolution exhibits stronger damping intensity and lower oscillation frequency, and the final equilibrium position significantly shifts towards that of the experimental result. Furthermore, when the influences of the DCA were taken into consideration, the amplitude of the free surface deflections was further damped. Figure 7 shows the evolution of contact angle adopting the DCA model in the $0g_0$ gravity condition. The DCA shows a damped oscillation synchronically with the evolution of MCL until reaching the SCA value where the contact line achieves its equilibrium position. Its discrepancy from SCA, i.e. $\theta_D - \theta_e$, approximately remains in the range of

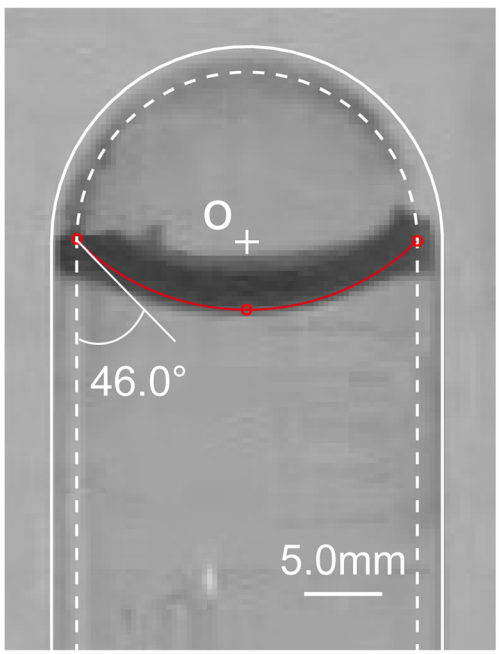

Fig. 6 Contact angle in the test tube

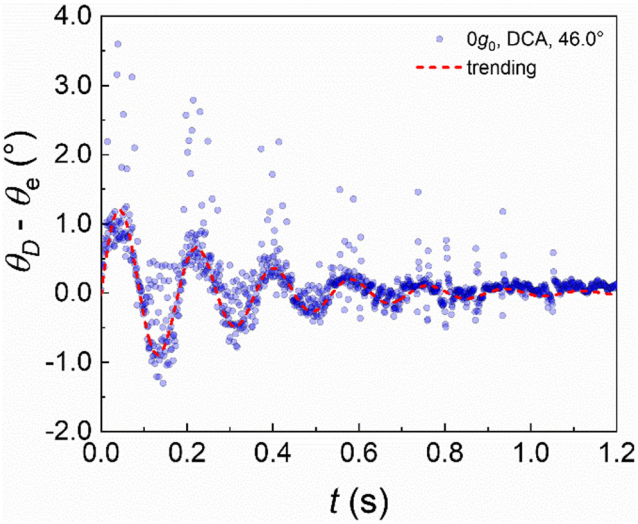

Fig. 7 Temporal evolution of the contact angle captured with the DCA model by Kistler (1993)

± 1.5 °. The free surface undergoes several oscillations and rapidly evolves into the equilibrium position due to the extra viscous damping on free surface oscillations. When the actual experimental gravity (i.e. g_R) condition was further considered, the evolution of the free surface deflections exhibits much stronger damping effect and much faster transition into the final equilibrium position after the initial maximum deflection. It is worth noting that the numerical result of the SCA model under the actual gravity level, as depicted in Fig. 5 (a), also exhibits stronger damping effect as compared with the result of SCA under g_S condition. Nevertheless, the numerical results of the evolution of FSC using DCA model (as shown in Fig. 5 (b)) agree better with the DTE result than the SCA model (as shown in Fig. 5 (a)) under g_R condition, especially after the first oscillation. Note that there is a space uncertainty of 0.3 mm in the image processing of the experimental results. As a result, the numerical result can be considered in a good agreement with the experimental results, which validates the present numerical simulation, supports the adoption of Kistler's DCA model and implies the importance of considering the actual gravity evolution in the experiment (Fig. 5).

Dependency of the Free Surface Dynamic Behaviors on the Air Fraction

It is worthwhile to figure out the dependency of the dynamic behavior of the free surfaces on air fraction k_v. Therefore, a series of numerical simulations were carried out for the dynamic behavior of the free surface under the step reduction gravity condition with k_v ranging from 0.80 to 1.88 in the tube. The results can be divided into three representative states regarding the position of the MCL, as shown in Fig. 8. S1 is for small k_v, e.g. 0.80, the contact line oscillation keeps staying over the horizontal plane of $z = 0$. S2 is for intermediate k_v, the contact line oscillates alternatively over and below the horizontal plane of $z = 0$. S3 is for large k_v, e.g. 1.88, the contact line oscillation keeps staying below the horizontal plane of $z = 0$.

Figure 9 compares the evolutions of the MCL and the FSC in the tube for air fraction k_v= 0.80, 1.30 and 1.88, which corresponds to three representative states of the contact line oscillations, S1, S2 and S3 (see Fig. 8), respectively. The dynamic evolution of MCL and FSC in $0g_0$ with SCA θ_e= 46.0° are also plotted as a comparison. For all the cases, after an abrupt drop of gravity, the evolutions of MCL and FSC reveal damped oscillations synchronously approaching to their respective equilibrium positions with a phase shift π. The final equilibrium position of MCL remains the same for both DCA and SCA, which

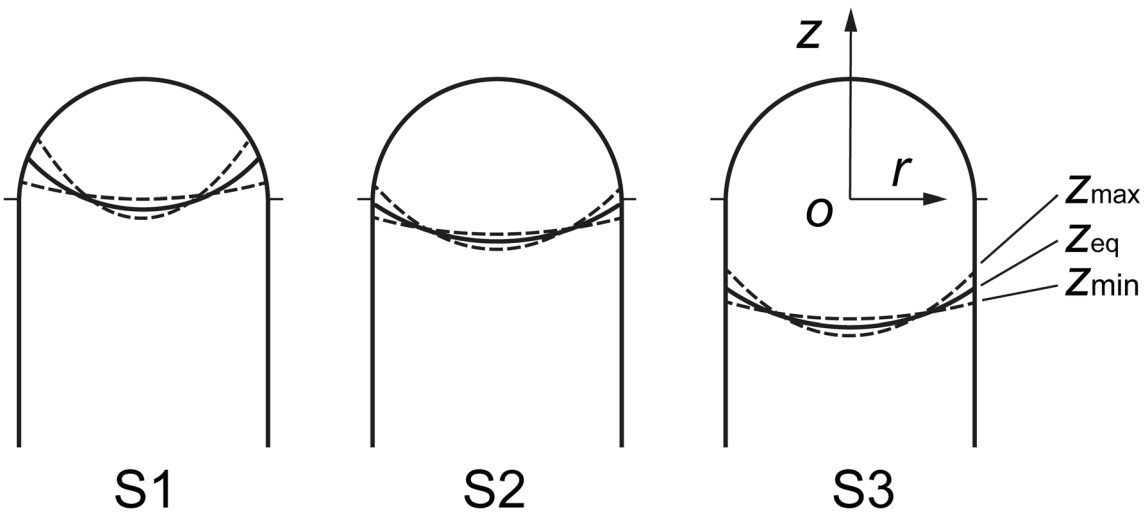

Fig. 8 Three representative states of the oscillations of contact line. Here z_{max}, z_{min} and z_{eq} represent the contact lines locating at the maximum, minimum and equilibrium position, respectively

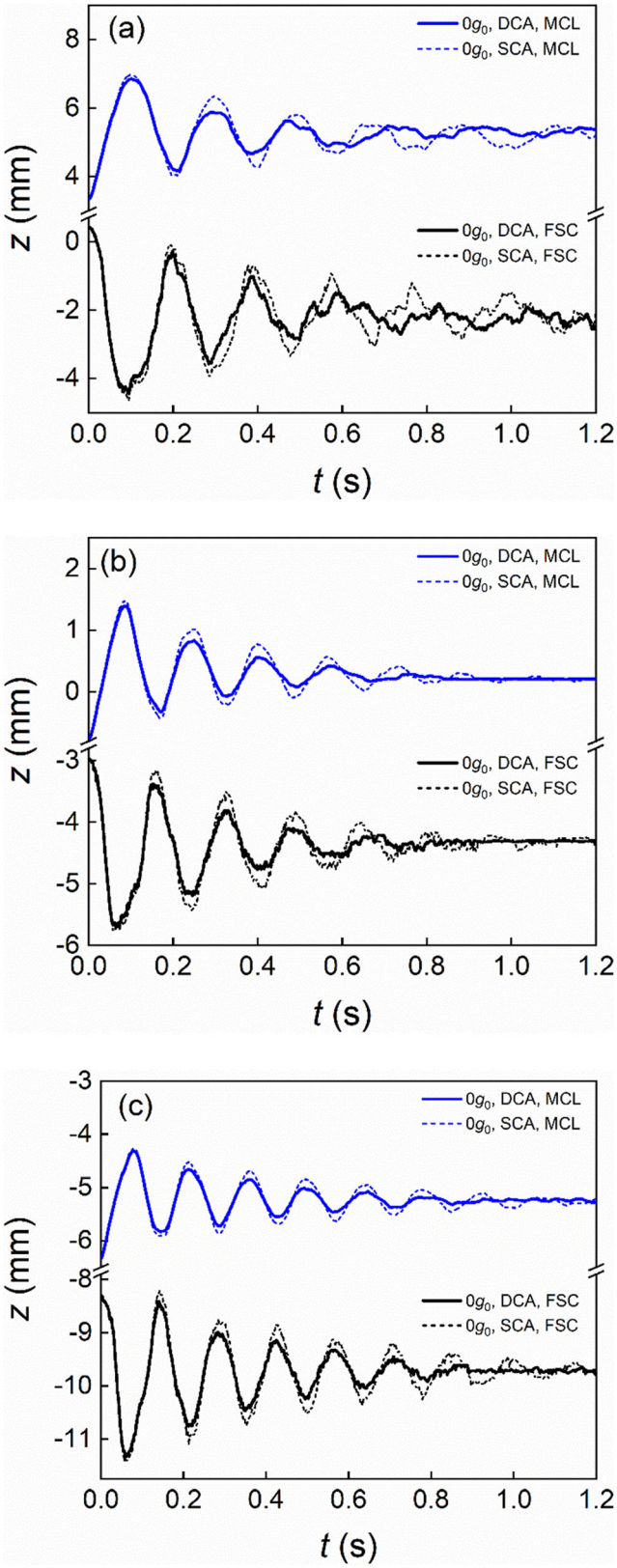

Fig. 9 Comparison of temporal evolution of the MCL and the FSC for different air fraction k_v after an abrupt drop of gravity. (a) k_v=0.80; (b) k_v= 1.30; (c) k_v= 1.88

means that the equilibrium position of MCL is determined by the value of SCA. The time duration required for a complete transition to the steady state in a reduced gravity condition is nearly the same for different values of k_v. However, the amplitude of the oscillation decreases with increasing k_v, which means larger damping intensity for smaller k_v. Notably, the amplitude of the MCL oscillation exhibits obvious discrepancies between the cases using DCA model and the cases using SCA model. In addition, there is a phase difference after the third period of MCL oscillations in the case of k_v= 0.80. However, this phase difference disappeared gradually as the case of k_v= 1.88 is approached. The principal reason for this phase difference lies still in the geometry of the physical model, in which the contact line moves with a curved path accounting for the spherical head of the tube in the case of k_v= 0.80, in contrast to a straight path for the cylindrical part in the case of k_v= 1.88. The analysis can be detailed as follows.

Without loss of generality, the evolution of the characteristic position of MCL and FSC can be specified by

$$z = Ae^{-\gamma t}\cos(\omega t - \phi), \tag{13}$$

where A is the amplitude, ϕ the initial phase, γ the relaxation frequency whose reciprocal $1/\gamma$ is the relaxation time in which the amplitude A is reduced by a factor of $1/e$, ω the angular frequency which is related to the frequency f by $\omega = 2\pi f$. The value of ω is

$$\omega = \sqrt{\omega_0^2 - \gamma^2}, \tag{14}$$

where ω_0 is the base angular frequency. From Eq. (14) we can see that a larger γ gives rise to a smaller ω.

Considering the relaxation frequency γ as a function of the characteristic length of the tube R, the density of liquid and gas ρ_l and ρ_g, the viscosity of liquid and gas μ_l and μ_g, the surface tension σ, the contact angle θ, and the gravity acceleration g, it has the following form:

$$\gamma = f\left(R; \rho_l, \rho_g, \mu_l, \mu_g, \sigma; \theta, g\right), \tag{15}$$

Taking R, ρ_l and σ as a unit system, Eq. (15) is reduced to a dimensionless relationship:

$$\gamma = t_c^{-1} f(Ca/Re, \theta, Bo), \tag{16}$$

where the Reynolds number is defined as $Re = \rho u R/\mu$. When it refers to the microgravity condition, the Bond number can be neglected, then Eq. (16) is reduced to

$$\gamma = t_c^{-1} f\left(Oh^2, \theta\right), \tag{17}$$

Table 1 Parameters of curve fitting of the MCL with the DCA model in $0g_0$, as Eq. (13) and (14) specified

k_v	A (mm)	γ (rad•s^{-1})	ω (rad•s^{-1})	ϕ (rad)	z_{eq} (mm)	ω_0 (rad•s^{-1})	γ/ω	R-square
0.80	2.018	3.442	30.950	3.190	5.274	31.141	0.111	0.846
1.30	1.231	3.790	37.450	9.544	0.282	37.641	0.101	0.919
1.88	1.025	2.960	43.950	9.328	−5.230	44.050	0.067	0.958

where the Ohnesorge number, specified by $Oh = \sqrt{Ca/Re} = \sqrt{\rho\nu^2/(\sigma R)}$, is a typical measurement of the damping effect (Stange et al. 2003), ν is the kinematic viscosity defined as $\nu = \mu/\rho$. From eq. (16) we can see that γ is proportional to the inverse of capillary time scale $t_c \sim \sqrt{\rho R^3/\sigma}$, which means a larger characteristic length referring to a smaller damping effect. On the other hand, the damping effect is the result of a competition between the capillary and viscosity effect, and the influence of contact angle. The specific form of Eq. (13) for the cases $k_v = 0.80$, 1.30, 1.88 was respectively figured out by curve fitting of the MCL data. The coefficient is bounded with the 95% confidence. As shown in Fig. 10, the numerical results of the oscillations of MCL exhibit good agreement with the theoretical predictions, except for the case of k_v=0.80 in which there are visible phase differences between the numerical and the theoretical results. The detailed fitting parameters are listed in Table 1.

As seen from Table 1, the damping intensity, specified by γ/ω, decreases from 0.111 to 0.067 as k_v increases from 0.80 to 1.88, which means the oscillation in the cylindrical part is subjected to a weaker damping effect. In the half-spherical part, the equivalent characteristic length $R^* < R$, leading to $t_c^* < t_c$. Therefore, the relaxation frequency γ for k_v = 0.80 is larger than that for k_v = 1.88. Notably, the relaxation frequency γ for k_v = 1.30 is slightly larger than that for k_v = 0.80. On one hand, this is partly due to the fact that z value of MCL was calculated by the z coordinate component in the Cartesian coordinate system rOz, as shown in Fig. 8. The actual distance of MCL in k_v = 0.80 is larger than what was displayed in Fig. 10 in every oscillation period. After correcting the z value of MCL to its actual distance in the cases of k_v = 0.80 and 1.30 (the corrected distances for the first half period take the value of Δz= 0.555 mm and 0.004 mm), the corrected relaxation frequencies are 3.450 and 3.779. On the other hand, the stronger damping effect of DCA for the case of k_v= 0.80 yields a larger time scale t_c as compared to the case of k_v= 1.30, which leads to a slight decrease in relaxation frequency γ.

Figure 11 describes the relationship between the oscillation frequencies of the meniscus and the air fractions in the tube. The oscillation frequency increases gradually with increasing k_v in the transition from state S1 to state S2. The increasing tendency becomes steeper in the further transition from state S2 to stateS3. In state S3, the oscillation frequency remains nearly constant with the increase of k_v. The trends of the oscillation frequency profiles for the cases with DCA and SCA models are qualitatively the same. However, visible

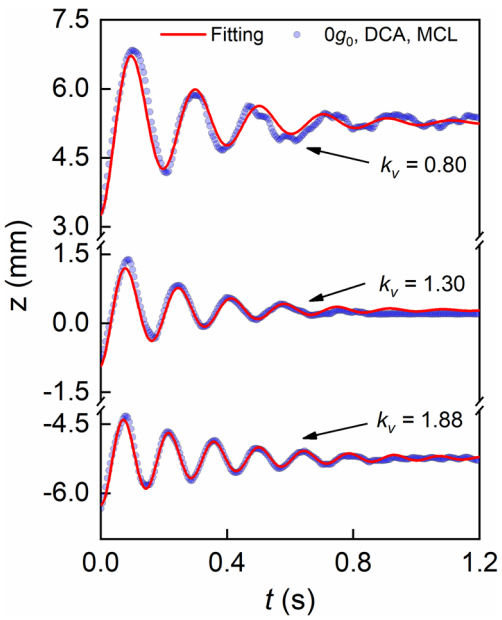

Fig. 10 Curve fitting results of MCL with the DCA model in $0g_0$ gravity condition for air fraction k_v of 0.80, 1.30, and 1.88

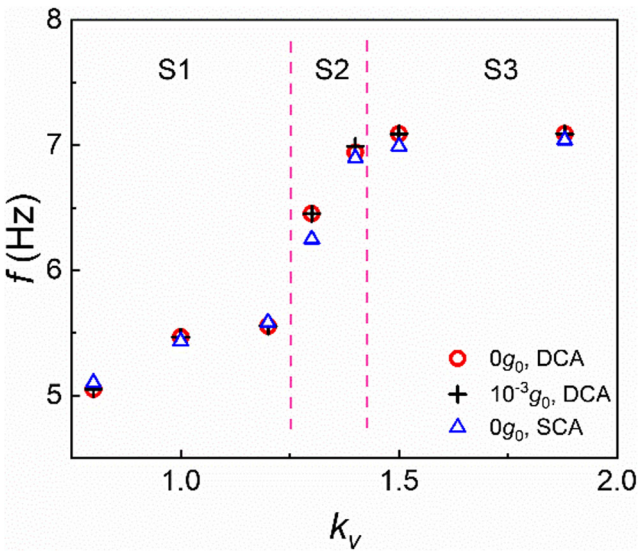

Fig. 11 Oscillation frequency of the evolution of free surface deflection vs. k_v

differences can be observed, especially in the air fraction region of S1. Therefore, to precisely predict the dynamic liquid behavior (sloshing). e.g. oscillation frequency and amplitude, in a partially filled storage tank which is dramatically larger than the present tube in geometry, it is necessary to take the DCA model into consideration. It is especially needed for the cases of small air fraction (large filling level) where the MCL remains in the spherical or ellipsoidal part of the tank. On the other hand, the residual gravity of $10^{-3}g_0$ exerts less influence on the oscillation frequency variation against the air fraction as compared to the present case.

Conclusions

The dynamic behavior of liquid in partially filled capsule storage tank in microgravity was investigated numerically based on the condition of Drop Tower Beijing experiment with DCA model taken into consideration. The VOF method was adopted to build the numerical model and to reveal more details of the liquid behavior, particularly the oscillation frequencies of the free surface. By incorporating the actual gravity condition of Drop Tower and the revised SCA into the simulation model, the numerical results shows good agreement with the experimental results, which indicates that the DCA model is more accurate and meaningful than the SCA model in the simulation of MCL problems. The dynamic behavior of two-phase free surface in step reduced gravity condition was investigated systematically, with the air fraction k_v in the tube ranging from 0.80 to 1.88. The results show that after an abrupt drop of gravity, the deflections of the free surface in tube reveal damping oscillations from its equilibrium position in normal gravity to its equilibrium position in microgravity. The oscillation amplitude decreases with the increase of air fraction k_v. The oscillation frequency increases with the increase of k_v while remaining nearly constant for large air fraction k_v, where the MCL stays on the cylindrical part of the tube. For the same k_v, the oscillation frequency significantly increases with decreasing tank diameter (Li et al. 2018). The dynamic behavior of free surfaces in the tube, i.e. the capsule tank, can be captured by the capillary theory with a time scale of $t_c \sim \sqrt{\rho R^3/\sigma}$. When the liquid sloshing in a storage tank is considered in microgravity condition, it is of crucial significance to take the DCA effect into account to predict the dynamic behavior of free surfaces, which is critical for the stability and safety of the whole system.

Acknowledgments This research is supported by the National Nature Science Foundation of China (Gant No. 11672311), the Strategic Project of Leading Science and Technology (Class A), CAS (Grant No. XDA15012700) and the Key Research Program of Frontier Sciences, CAS (Grant No. QYZDY-SSW-JSC040).

References

Almohammadi, H., Amirfazli, A.: Droplet impact: viscosity and wettability effects on splashing. J. Colloid Interface Sci. **553**, 22–30 (2019). https://doi.org/10.1016/j.jcis.2019.05.101

Barsi, S., Kassemi, M.: Investigation of tank pressurization and pressure control—part I: experimental study. Journal of Thermal Science and Engineering Applications. **5**(4), 041005 (2013). https://doi.org/10.1115/1.4023891

Blake, T.D., Batts, G.N.: The temperature-dependence of the dynamic contact angle. J. Colloid Interface Sci. **553**, 108–116 (2019). https://doi.org/10.1016/j.jcis.2019.06.006

Brackbill, J.U., Kothe, D.B., Zemach, C.: A continuum method for modeling surface tension. J.comp.phys. **100**(2), 335–354 (1992)

Chang, S., Ding, L., Song, M., Leng, M.: Numerical investigation on impingement dynamics and freezing performance of micrometer-sized water droplet on dry flat surface in supercooled environment. Int. J. Multiphase Flow. **118**, 150–164 (2019). https://doi.org/10.1016/j.ijmultiphaseflow.2019.06.011

Chen, L., Liang, G.-Z.: Simulation research of vaporization and pressure variation in a cryogenic propellant tank at the launch site. Microgravity Science and Technology. **25**(4), 203–211 (2013). https://doi.org/10.1007/s12217-013-9340-2

Cox, R.G.: The dynamics of the spreading of liquids on a solid surface. Part 1. Viscous flow. J. Fluid Mech. **168**, 169–194 (1986). https://doi.org/10.1017/S0022112086000332

Dalmon, A., Lepilliez, M., Tanguy, S., Alis, R., Popescu, E.R., Roumiguié, R., Miquel, T., Busset, B., Bavestrello, H., Mignot, J.: Comparison between the FLUIDICS experiment and direct numerical simulations of fluid sloshing in spherical tanks under microgravity conditions. Microgravity Science and Technology. **31**(1), 123–138 (2019). https://doi.org/10.1007/s12217-019-9675-4

Dalmon, A., Lepilliez, M., Tanguy, S., Pedrono, A., Busset, B., Bavestrello, H., Mignot, J.: Direct numerical simulation of a bubble motion in a spherical tank under external forces and microgravity conditions. J. Fluid Mech. **849**, 467–497 (2018). https://doi.org/10.1017/jfm.2018.389

Deng, M.L., Yue, B.Z.: Attitude tracking control of flexible spacecraft with large amplitude slosh. Acta Mech. Sinica. **33**(6), 1095–1102 (2017). https://doi.org/10.1007/s10409-017-0700-9

Fernandez, J., Sanchez, P.S., Tinao, I., Porter, J., Ezquerro, J.M.: The CFVib experiment: control of fluids in microgravity with vibrations. Microgravity Science and Technology. **29**(5), 351–364 (2017). https://doi.org/10.1007/s12217-017-9556-7

Fricke, M., Koehne, M., Bothe, D.: A kinematic evolution equation for the dynamic contact angle and some consequences. Physica D-Nonlinear Phenomena. **394**, 26–43 (2019). https://doi.org/10.1016/j.physd.2019.01.008

Fries, N., Dreyer, M.: An analytic solution of capillary rise restrained by gravity. J. Colloid Interface Sci. **320**(1), 259–263 (2008). https://doi.org/10.1016/j.jcis.2008.01.009

Gueyffier, D., Li, J., Nadim, A., Scardovelli, R., Zaleski, S.: Volume-of-fluid interface tracking with smoothed surface stress methods for three-dimensional flows. J. Comput. Phys. **152**(2), 423–456 (1999)

Hirt, C.W., Nichols, B.D.: Volume of fluid (VOF) method for the dynamics of free boundaries. J. Comput. Phys. **39**(1), 201–225 (1981)

Ho, S., Rahman, M.: Three-dimensional analysis of liquid hydrogen cryogenic storage tank. Paper presented at the 3rd International Energy Conversion Engineering Conference, AIAA 2005–5712 (2005). https://doi.org/10.2514/6.2005-5712

Hoffman, R.L.: A study of the advancing interface. I. Interface shape in liquid—gas systems. Journal of Colloid & Interface Science. **50**(2), 228–241 (1975)

Jiang, T.S., Soo-Gun, O.H., Slattery, J.C.: Correlation for dynamic contact angle. Journal of Colloid & Interface Science. **69**(1), 74–77 (1979)

Josserand, C., Thoroddsen, S.T.: Drop impact on a solid surface. Annu. Rev. Fluid Mech. **48**(1), 365–391 (2016). https://doi.org/10.1146/annurev-fluid-122414-034401

Kassemi, M., Kartuzova, O.: Effect of interfacial turbulence and accommodation coefficient on CFD predictions of pressurization and pressure control in cryogenic storage tank. Cryogenics. **74**, 138–153 (2016). https://doi.org/10.1016/j.cryogenics.2015.10.018

Kistler, S.F.: Hydrodynamics of wetting. in Wettability, edited by J. C. Berg (Marcel Dekker, New York, 1993), p.311 (1993)

Kulev, N., Dreyer, M.: Drop tower experiments on non-isothermal reorientation of cryogenic liquids. Microgravity Science and Technology. **22**(4), 463–474 (2010). https://doi.org/10.1007/s12217-010-9237-2

Kumar, S.P., Prasad, B.V.S.S.S., Venkatarathnam, G., Ramamurthi, K., Murthy, S.S.: Influence of surface evaporation on stratification in liquid hydrogen tanks of different aspect ratios. Int. J. Hydrog. Energy. **32**(12), 1954–1960 (2007). https://doi.org/10.1016/j.ijhydene.2006.08.052

Li, J.C., Lin, H., Zhao, J.F., Li, K., Hu, W.R.: Dynamic behaviors of liquid in partially filled tank in short-term microgravity. Microgravity Science and Technology. **30**(6), 849–856 (2018). https://doi.org/10.1007/s12217-018-9642-5

Li, Y.Q., Cao, W.H., Liu, L.: Numerical simulation of capillary flow in fan-shaped asymmetric interior corner under microgravity. Microgravity Science and Technology. **29**, 65–79 (2017). https://doi.org/10.1007/s12217-016-9526-5

Liang, G., Mudawar, I.: Review of drop impact on heated walls. Int. J. Heat Mass Transf. **106**, 103–126 (2017). https://doi.org/10.1016/j.ijheatmasstransfer.2016.10.031

Lopez, A., Grayson, G., Chandler, F., Hastings, L., Hedayat, A.: Cryogenic Pressure Control Modeling for Ellipsoidal Space Tanks. Paper presented at the 43rd AIAA/ASME/SAE/ASEE Joint Propulsion Conference & Exhibit (2007)

Lopez, A., Grayson, G., Chandler, F., Hastings, L., Hedayat, A.: Cryogenic Pressure Control Modeling for Ellipsoidal Space Tanks in Reduced Gravity. Paper presented at the 44th AIAA/ASME/SAE/ASEE Joint Propulsion Conference & Exhibit (2008)

Park, J., Im, S., Sung, H.J., Park, J.S.: PIV measurements of flow around an arbitrarily moving free surface. Exp. Fluids. **56**(3), 56 (2015). https://doi.org/10.1007/s00348-015-1920-z

Quetzeri-Santiago, M.A., Castrejon-Pita, A.A., Castrejon-Pita, J.R.: The effect of surface roughness on the contact line and splashing dynamics of impacting droplets. Sci. Rep. **9**(1), 15030 (2019). https://doi.org/10.1038/s41598-019-51490-5

Salgado Sanchez, P., Fernandez, J., Tinao, I., Porter, J.: Vibroequilibria in microgravity: comparison of experiments and theory. Phys. Rev. E. **100**, 063103 (2019). https://doi.org/10.1103/PhysRevE.100.063103

Snoeijer, J.H., Andreotti, B.: Moving contact lines: scales, regimes, and dynamical transitions. Annu. Rev. Fluid Mech. **45**(1), 269–292 (2013). https://doi.org/10.1146/annurev-fluid-011212-140734

Stange, M., Dreyer, M.E., Rath, H.J.: Capillary driven flow in circular cylindrical tubes. Phys. Fluids. **15**(9), 2587–2601 (2003). https://doi.org/10.1063/1.1596913

Sui, Y., Ding, H., Spelt, P.D.M.: Numerical simulations of flows with moving contact lines. Annu. Rev. Fluid Mech. **46**(1), 97–119 (2014). https://doi.org/10.1146/annurev-fluid-010313-141338

Sussman, M., Smereka, P., Osher, S.: A level set approach for computing solutions to incompressible two-phase flow. J. Comput. Phys. **114**(1), 146–159 (1994). https://doi.org/10.1006/jcph.1994.1155

Utsumi, M.: Slosh damping caused by friction work due to contact angle hysteresis. AIAA J. **55**(1), 265–273 (2017). https://doi.org/10.2514/1.j055238

Viola, F., Brun, P.T., Gallaire, F.: Capillary hysteresis in sloshing dynamics: aweakly nonlinear analysis. J. Fluid Mech. **837**, 788–818 (2018). https://doi.org/10.1017/jfm.2017.860

Vreeburg, J.P.B.: Simulation of liquid dynamics onboard Sloshsat FLEVO. AIP Conference Proceedings. **458**, 836 (1999). https://doi.org/10.1063/1.57704

Wang, X., Zhou, B., Jiang, M.: Technical challenges in numerical simulation of droplet behaviors with dynamic contact angle in microchannels. Int. J. Energy Res. **43**(9), 4828–4839 (2019). https://doi.org/10.1002/er.4633

Yang, W.J., Zhang, T.T., Li, C., Li, S.M., Xu, X.H.: Numerical Simulation of Pitching Sloshing under Microgravity. J. Appl. Fluid Mech. **12**(5), 1527–1537 (2019). https://doi.org/10.29252/jafm.12.05.29677

Youngs, D.L.: Time-Dependent Multi-material Flow with Large Fluid Distortion. Academic Press, pp.273–285 (1982)

Zhou, X., Liu, Z., Huai, X.: Evolution of free surface in the formation of thermo-Solutocapillary convection within an open cavity. Microgravity Science and Technology. **28**(4), 421–430 (2016). https://doi.org/10.1007/s12217-016-9492-y

Zhou, Z., Huang, H.: Constraint surface model for large amplitude sloshing of the spacecraft with multiple tanks. Acta Astronaut. **111**, 222–229 (2015)

Zwicke, F., Eusterholz, S., Elgeti, S.: Boundary-conforming free-surface flow computations: Interface tracking for linear, higher-order and isogeometric finite elements. Comput. Methods Appl. Mech. Eng. **326**, 175–192 (2017). https://doi.org/10.1016/j.cma.2017.08.022